Schindler, H. D., and R. E. Treybal, "Continuous-Phase Mass-Transfer Coefficients for Liquid Extraction in Agitated Vessels," *ibid.*, 790 (1968).
Treybal, R. E., *Liquid Extraction*, 2 ed., McGraw-Hill, New York (1963).
Yeheskel, J., and E. Kehat, "Wake Phenomena in a Liquid-Liquid Fluidized Bed," *AIChE J.*, **19**, 729 (1973).

Manuscript received November 15, 1977; revision received May 30, and accepted June 21, 1978.

A Comprehensive Experimental Investigation of Tubular Entry Flow of Viscoelastic Fluids.

Part II. The Velocity Field in Stable Flow

P. J. CABLE
Department of Chemical Engineering
Monash University
Clayton, Victoria, Australia
and D. V. BOGER
Department of Chemical Engineering
University of Delaware
Newark, Delaware

Center-line velocities and developing velocity profiles are presented for viscoelastic fluids flowing in a 2:1 and 4:1 abrupt entry contraction. Two flow regimes are clearly identified: a vortex growth regime and a divergent flow regime. Dramatic differences in the velocity field are observed and discussed for the two flow regimes. A kinematic model based on the velocity field data is proposed for vortex growth flow.

VELOCITY PROFILE MEASUREMENT

In parallel with the determination of the vortex characteristic discussed in Part I, point velocity measurement were made in the region just upstream of the 4:1 and 2:1 contractions. Of interest was the development of the axial velocity at the tube center line and the rearrangement of the axial velocity profile across the tube radius in the entry flow region, for both the vortex growth and the divergent flow regimes.

The two test sections used in the work were designed with long calming lengths upstream of the contraction plane to allow for dissipation of upstream disturbances before the fluid entered the contraction. To make sure that no disturbances were present, the axial velocity profile well upstream of each contraction was measured and compared with the theoretical fully developed profile. The accuracy of point velocity measurements was also checked by numerically integrating the velocity-radial position profiles and comparing the result with the separately measured volumetric flow rate. In all cases, the experimental profiles well upstream agreed to with 5% of the theoretical fully developed profiles, and the volumetric flow rate found by profile integration was within ±2% of the independently measured fluid flow rate.

The experimental conditions at which velocity measurements were made are summarized in Table 1. The parameters are calculated at the wall shear rate for fully developed flow in the downstream tube. Cases V1.1, V3.1, and V3.2 are in the vortex growth region, whereas V1.2, V1.3, V3.3, and V3.4 are in the divergent flow regime (see Figures 7, 8, and 11 in Part I). In general, the presentation of results which follows will differentiate between these two regions in order to establish the kinematic characteristics of each.

CENTER-LINE VELOCITY PROFILES

The development of the axial velocity at the tube center line from the upstream fully developed region to the contraction plane is shown in Figure 1 for fluid V3 in the 4:1 geometry. The axial velocity is shown in dimensionless form with respect to the average upstream velocity. In the vortex growth regime (V3.1, V3.2), for $N'_{Re} < 20$ and $N_{WS} < 0.5$, the axial velocity

Correspondence concerning this paper should be addressed to D. V. Boger, Monash University, Clayton, Victoria, Australia. P. J. Cable is with ICI Australia, Limited, Ascot Vale, Victoria, Australia.

Part I of this paper was published in the *AIChE J.* **24**, No. 5, 869 (1978).
Part III is scheduled for publication in the *AIChE J.* **25**, No. 1. (1979).
0001-1541-78-1535-0992-$01.05.

TABLE 1. EXPERIMENTAL CONDITIONS FOR POINT VELOCITY MEASUREMENTS IN BOTH CONTRACTIONS FOR FLUIDS V1 AND V3

	2:1 Contraction			4:1 Contraction			
Run No.	V1.1	V1.2	V1.3	V3.1	V3.2	V3.3	V3.4
$\langle v_z \rangle_d$ (m/s)	0.121	0.152	0.422	0.324	0.549	1.21	1.95
$\dot{\gamma}_w$ (s^{-1})	51.3	64.5	180	266	448	994	1 610
N_1/τ	6.01	6.38	8.34	9.20	11.2	13.7	15.8
θ_w (s)	5.9×10^{-2}	5.0×10^{-2}	2.3×10^{-2}	1.73×10^{-2}	1.25×10^{-2}	6.87×10^{-3}	4.90×10^{-3}
N'_{Re}	4.71	6.71	33.5	6.84	15.3	59.6	132
N_{WS}	0.280	0.296	0.386	0.393	0.479	0.581	0.670

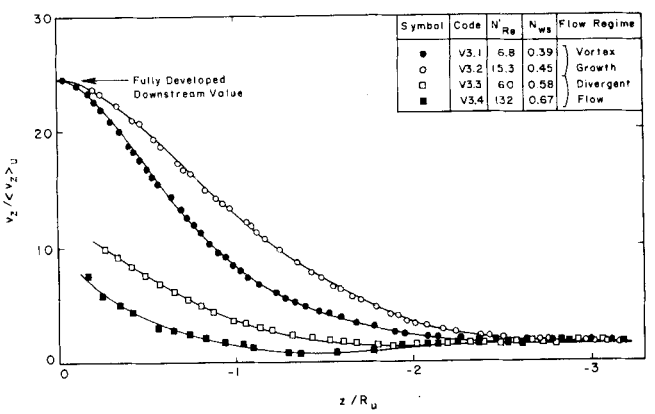

Fig. 1. Center-line velocity profiles in the entry region of the 4:1 contraction for fluid V3.

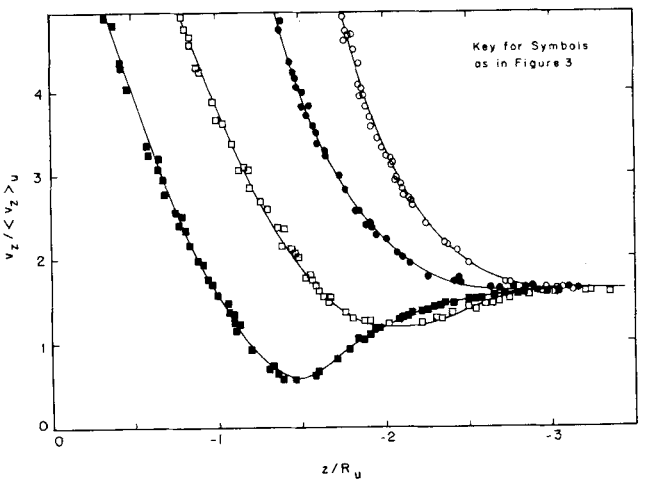

Fig. 2. Center-line velocity profiles in the entry region of the 4:1 contraction for fluid V3: detailed comparison of the lower velocity range.

at the center line increases monotonically as the contraction plane is approached. At $N'_{Re} = 6.8$ and $N_{WS} = 0.39$ (V3.1), the fluid begins to accelerate at approximately two and one fourth large tube radii upstream of the contraction plane, and the center-line velocity equals its fully developed downstream value at the small tube entrance. All the velocity profile rearrangement occurs in the upstream tube region. The vortex detachment plane is located at $z/R_u = -1.74$, whereas fluid acceleration can be seen to begin at $z/R_u \simeq -2.3$. The fluid begins to accelerate before the detachment plane is reached owing to large axial normal stresses at the center line.

At higher flow rates within the vortex growth region, the predevelopment of the center-line velocity is enhanced owing to the larger secondary vortex and greater tensile elastic stresses at the center line. This is shown in Figure 1 for V3.2 at $N'_{Re} = 15.3$ and $N_{WS} = 0.45$. Acceleration begins almost three large tube radii upstream of the contraction plane, and the velocity profile at the entrance to the small tube is still essentially fully developed.

In the divergent flow regime, the nature of the center-line velocity development changes significantly. Figure 1 shows the behavior which occurs once the point of maximum vortex size is passed for V3.3 and V3.4 at $N'_{Re} = 60$, 132 and $N_{WS} = 0.58$, 0.67. Fluid particles at the center line decelerate before the detachment plane is reached. This is to be expected, since flow pattern observations have shown that the flow diverges from the center line in this region (Figure 8 in Part I). It may also be inferred from Figure 1 that the velocity profile at the entrance is no longer fully developed in the divergent flow regime. It would appear that the profile has become more uniform, or flatter, as the flow rate increases.

A more detailed comparison of the four center-line velocity profiles is given in Figure 2 for values of the dimensionless center line axial velocity less than five units. The marked deceleration in V3.3 and V3.4 is evident, especially at $N'_{Re} = 130$ ($N_{WS} = 0.67$), where the axial velocity at the center line decreases to one third of its upstream fully developed value, at $z/R_u = -1.5$, before acceleration begins.

An alternative method of inspecting the center-line velocity profiles is to normalize the point velocities with respect to the average velocity at the appropriate axial position. Referring to Figure 6 in Part I, the axial velocity at the center line may be normalized as follows:

$$\left.\begin{aligned} &\text{for } z \leq -L_v, && v_z|_N = \frac{v_z}{\langle v_z \rangle_u} \\ &\text{for } -L_v \leq z \leq 0, && v_z|_N = \frac{v_z}{\langle v_z \rangle_v} \\ &\text{for } z \geq 0, && v_z|_N = \frac{v_z}{\langle v_z \rangle_d} \end{aligned}\right\} \quad (1)$$

Here $\langle v_z \rangle_v$ is the average velocity in the vortex region, which can be expressed in terms of the average downstream velocity by

$$\langle v_z \rangle_v = \frac{R_d^2}{R_v^2} \langle v_z \rangle_d \quad (2)$$

$\langle v_z \rangle_v$ is a function of z. The advantage of this method of visualizing the center-line velocity profiles is that it emphasizes the profile rearrangements and removes the effect of the acceleration due to the reduction in tube cross section. For example, if the velocity profile main-

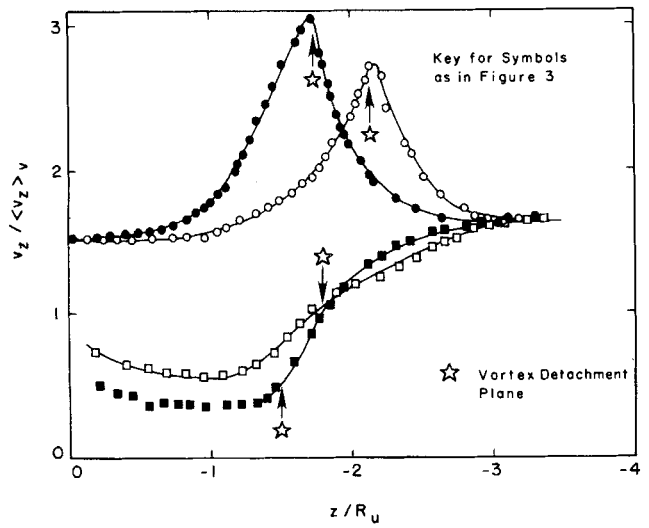

Fig. 3. Normalized center-line velocity profiles in the entry region of the 4:1 contraction for fluid V3, showing also the location of the vortex detachment plane.

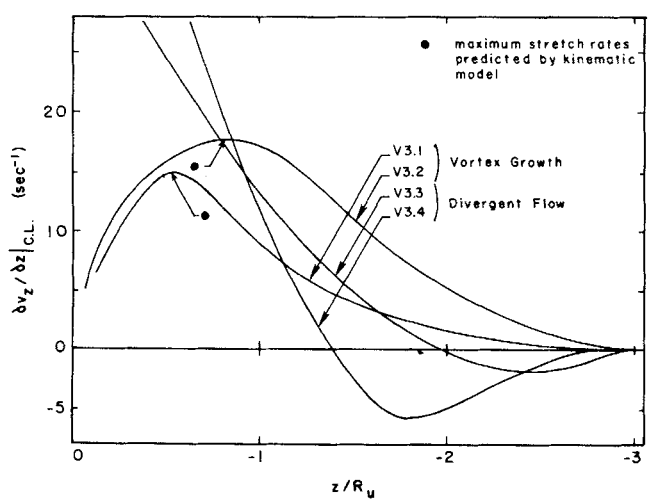

Fig. 4. Center-line stretch rates in the entry region of the 4:1 contraction for fluid V3.

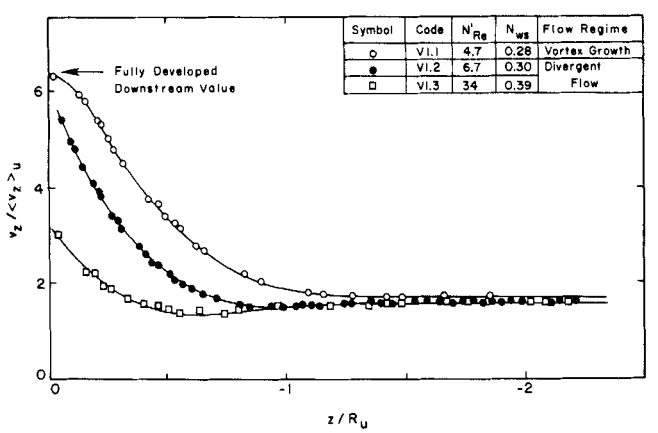

Fig. 5. Center-line velocity profiles in the entry region of the 2:1 contraction for fluid V1.

tained a constant shape through the entry region, such as the fully developed shape, then a graph of $v_z|_N$ against z, at the center line, would be a horizontal line, indicating that no profile rearrangement occurs in the entry region. This normalization method will also be applied shortly when the variation of axial velocity profiles across the tube radius, through the entry region, is considered.

The center-line velocity profiles for fluid V3 in the 4:1 entry region are presented in normalized form in Figure 3, as $v_z|_N$ vs. z/R_u. The location of the vortex detachment plane for each case is indicated by a star. For the two profiles obtained in the vortex growth region (V3.1, V3.2), significant predevelopment of the center-line velocity occurs before the detachment plane is reached. For the lowest Reynolds number, the normalized center-line velocity approaches twice its upstream fully developed value. Within the vortex region, the normalized profile begins to relax back to its fully developed form, reaching this condition as the small tube entrance is approached. In contrast, the marked deceleration in the divergent flow regime persists within the vortex region, where the normalized center-line velocity maintains a low value before rapid acceleration finally sets in near the contraction plane.

Extensional rates at the tube center line $\partial v_z/\partial z$ were estimated for the four cases studied from lines of best fit through the data in Figures 1 and 2. The center line stretch rate was then obtained by multiplying the resultant dimensionless gradient by $\langle v_z \rangle_u / R_u$. The results are presented as approximate curves in Figure 4. For the vortex growth regime, the stretch rate is zero for $z/R_u \leq -3$, increases monotonically to a maximum somewhere between the vortex detachment and contraction planes, and decreases to zero at the small tube entrance. The maximum value increases with flow rate, being about 15 s^{-1} for V3.1, and 18 s^{-1} for V3.2. A distinct contrast is obtained in the divergent flow regime. Starting at zero well upstream, the stretch rate becomes negative, decreasing to a minimum near the detachment plane. It then increases, passing through zero and becoming apparently quite large (greater than 25 s^{-1}) as the con-

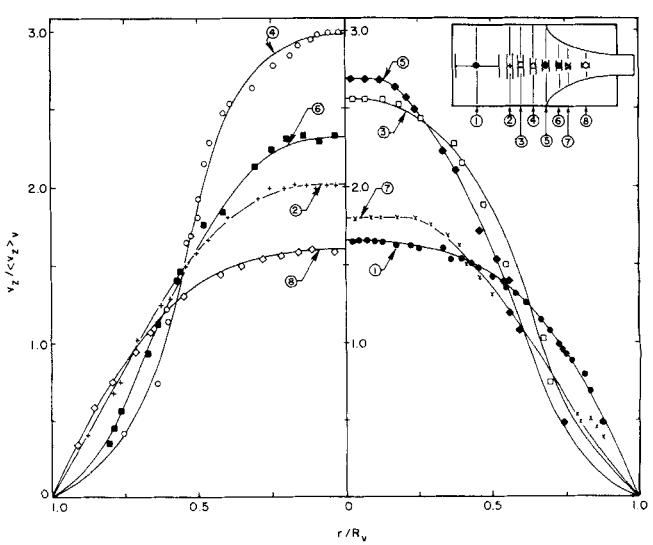

Fig. 6. Developing axial velocity profiles in the entry region of the 4:1 contraction for fluid V3, case V3.4 ($N_{RE}' = 130$, $N_{WS} = 0.67$, vortex growth regime). Data normalized to account for secondary vortex.

traction plane is approached. Unfortunately, reliable data in the high velocity region just upstream of the small tube entrance were not obtainable, and quantitative information about the stretch rates in this region at high velocities is not available. Also shown in Figure 4 are two data points representing estimated values for the stretch rates for V3.1 and V3.2, using a kinematic model which will be developed shortly.

Similar effects to those established for the 4:1 contraction were observed for fluid V1 in the 2:1 geometry. Figure 5 shows the dimensionless center-line velocity variation with axial distance, upstream of the 2:1 entrance, for three flow rates. Case V1.1 is in the vortex growth region, with $N'_{Re} = 4.7$, $N_{WS} = 0.28$, and the velocity profile in Figure 5 shows the established characteristics of the vortex growth region, with smooth acceleration occurring to give fully developed flow at the small tube entrance. Cases V1.2 and V1.3 are in the divergent flow regime with $N'_{Re} = 6.7$ and 34, and $N_{WS} = 0.30$ and 0.39, respectively. The divergent flow profiles in Figure 5 exhibit slight deceleration at the center line, becoming more pronounced with increasing flow rate. The entrance velocity profile becomes more uniform at the same time. Comparison of these center-line velocity profiles with those of RamaMurthy (1970) yields qualitative agreement on the trends observed.

AXIAL VELOCITY PROFILE REARRANGEMENTS

This section will establish the manner in which the axial velocity profile across the tube radius alters as the fluid flows through the entry region. As before, the axial velocity is made dimensionless using Equation (1). Similarly, the radial coordinate is normalized by dividing by R_u upstream of the detachment plane and R_v in the vortex region ($-L_v < z < 0$). In order to characterize the profile rearrangements, extensive point velocity measurements were made for fluid V3 in the 4:1 contraction, where the effects were more readily established than in the 2:1 geometry.

Vortex Growth Regime

The variation in the axial velocity profile as the fluid flows through the entry region is shown in Figure 6 for fluid V3 at $N'_{Re} = 6.8$, $N_{WS} = 0.39$ (V3.1). The data are presented as a set of profiles at various axial positions, axial velocity being plotted against radial position. The axes are normalized as described above, accounting for the presence of the secondary vortex. Each profile is presented for half the tube only, the other half being a symmetrical mirror image. Profiles at successive axial positions are shown on alternative sides of the graph in order to delineate the profile rearrangement more clearly. The axial positions for each of the eight profiles are also indicated in the small sketch of the entry flow field at the top of the graph to show their location in relation to the vortex detachment and contraction planes.

Well upstream of the contraction the flow is fully developed (profile 1 in Figure 6). As the detachment plane is approached (profiles 2, 3, 4), the velocity at the center line increases, while fluid particles near the wall decelerate. The velocity profile may be visualized as overdeveloped. Within the vortex region ($-L_v \leq z \leq 0$), the shape of the profile rounds out as the contraction plane is approached (profiles 5, 6, 7). Approaching the small tube entrance, the profile becomes identical in shape to the downstream fully developed form (profile 8). The flow is fully developed entering the small tube.

Summarizing the kinematic characteristics of vortex growth, the velocity profile overdevelops as the detachment plane is approached. The center-line velocity becomes almost twice the fully developed upstream value. In the vortex region, the velocity profile changes shape in the reverse manner, relaxing to become fully developed again near the contraction plane. At the same time acceleration occurs, so that the mean velocity increases sixteenfold between the vortex detachment plane and the small tube entrance. This effect has been removed from Figure 6 by the normalization of the point velocities and radial positions.

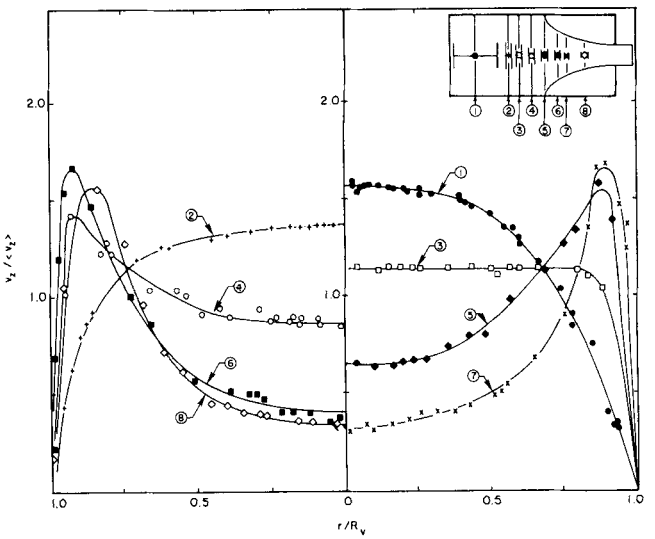

Fig. 7. Developing axial velocity profiles in the entry region of a 4:1 contraction for fluid V3, case V3.4 ($N_{RE}' = 130$, $N_{WS} = 0.67$, divergent flow regime). Data normalized to account for secondary vortex.

Inspection of the axial velocity profiles in the entry region at higher flow rates in the vortex growth regime (V3.2) yields little new information. The profile rearrangement begins further upstream, as suggested by the center-line velocity profiles in Figure 1. Approximately the same degree of overdevelopment occurs at the detachment plane, and the flow is fully developed at the small tube entrance. The latter point justifies, in part, the use of downstream fully developed conditions to correlate the entry flow behavior. In particular, the wall shear rate at the sharp edged corner of the entrance is a suit-

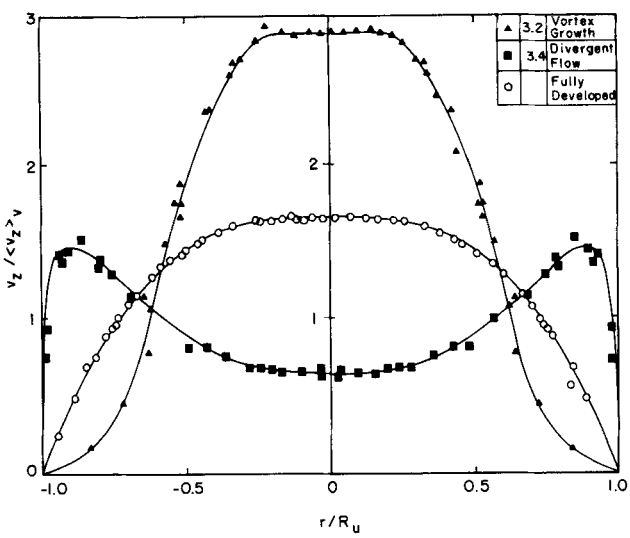

Fig. 8. Normalized axial velocity vs. radial position at the vortex detachment plane in the 4:1 contraction for cases V3.2 and V3.4, compared with the upstream fully developed profile.

able basis for the calculation of dimensionless groups to characterize the flow.

Divergent Flow

Axial velocity profiles in the entry region for fluid V3 at $N'_{Re} = 130$, $N_{WS} = 0.67$ (V3.4 — divergent flow) are given in Figure 7. The profiles were again symmetrical, and alternate sides of the graph are used at successive axial positions. It is seen that the significant deceleration at the center line, which was shown in Figure 2, is accompanied by acceleration of fluid particles near the well, resulting in velocity profiles of a most unusual shape.

Starting from fully developed flow well upstream (profile 1 in Figure 7), the velocity profile gradually flattens out (profiles 2 and 3) and becomes concave (profiles 4 and 5) as the detachment plane is approached. Large maxima in the axial velocity occur near the tube wall, the peak value being almost three times the local minimum at the tube center line. This effect becomes even more pronounced as the fluid enters the vortex region (profiles 6 and 7). On nearing the contraction plane, the velocity profile flattens out slightly (profile 8). The data in the close vicinity of the contraction plane were not sufficiently reliable to allow the entry profile to be specified. It is reasonable to presume from the center-line velocity profile in Figure 1 and the developing profiles in Figure 7 that the axial velocity profile at the entrance is approaching a uniform shape. This is significantly different from the fully developed condition in the vortex growth regime.

Similar phenomena were observed at lower flow rates in the divergent flow regime, for $N'_{Re} = 60$ and $N_{WS} = 0.58$ (V3.3), but the deceleration of fluid particles at the center line is not so pronounced, and the off-center maxima in the axial velocity are nearer the tube center line and smaller in magnitude.

The marked difference between the vortex growth and divergent flow regimes may be emphasized by comparing the normalized axial velocity profiles at the vortex detachment plane. Figure 8 shows these profiles for case V3.2 ($N'_{Re} = 15.3$, $N_{WS} = 0.48$) in the vortex growth regime and case V3.4 ($N'_{Re} = 132$, $N_{WS} = 0.67$) in the divergent flow regime. Also shown is the fully developed upstream axial velocity profile. The considerable overdevelopment of the profile in the vortex growth regime is in striking contrast to the concave profile in the divergent flow condition. Both the detachment plane profiles shown in Figure 8 gave excellent agreement with the independently measured volumetric flow rate on integration as $v_z \cdot r$ vs. r, as indeed did all the velocity profiles shown in Figures 6 and 7.

It is relatively simple to postulate a mechanism for the velocity profile rearrangements in the vortex growth regime. Large axial normal stresses at the tube center line cause acceleration of fluid particles before the vortex detachment plane is reached. In order to maintain continuity, fluid near the wall decelerates. The resultant velocity profile at the detachment plane is overdeveloped, as shown in Figure 8. More figuratively, highly deformed fluid flowing into the downstream tube drags fluid from the upstream reservoir after it.

The origin of the unusual effects in the divergent flow regime is more difficult to establish. It has already been found from the study of vortex characteristics that in the divergent flow regime the vortex decreases in size with increasing flow rate, due to increased fluid inertia. It is not clear, however, what causes the deceleration of fluid particles at the center line. It is almost as though the fluid is confronted by an invisible obstacle upstream of the small tube entrance and is forced to flow around it, resulting in divergent flow and velocity maxima near the tube wall.

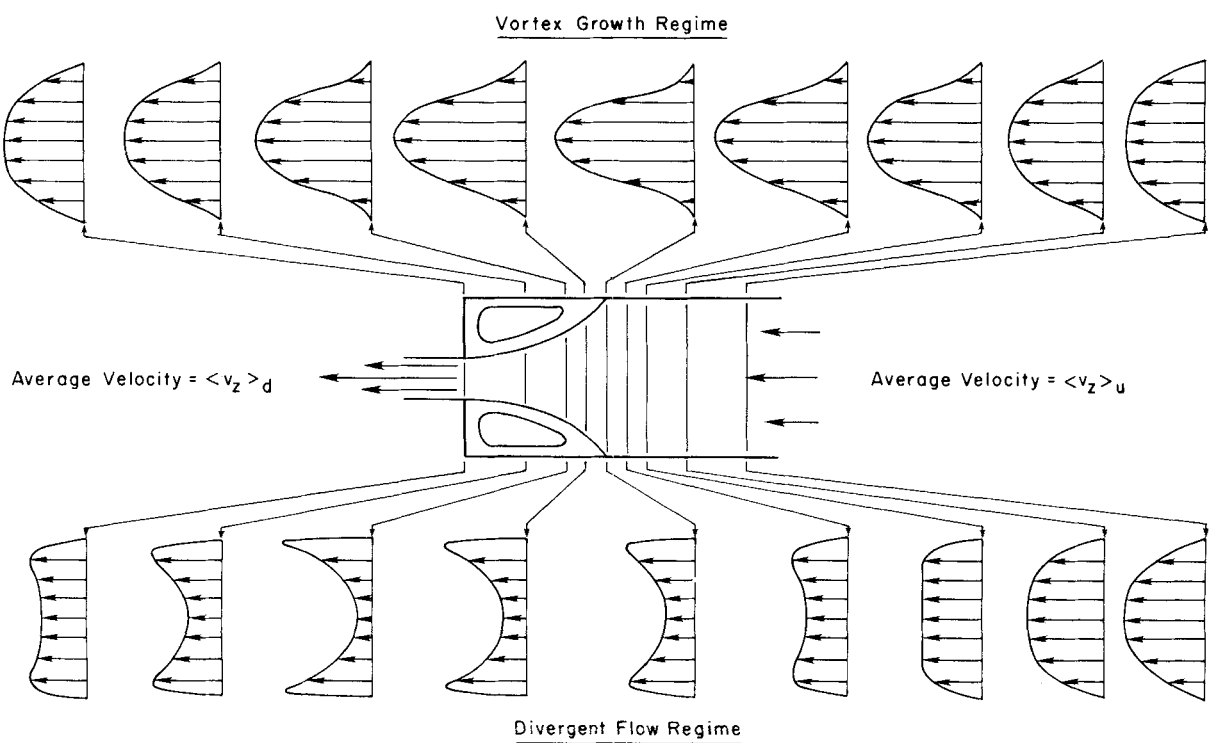

Fig. 9. Qualitative comparison of the normalized axial velocity profile rearrangements in the entry region for the vortex growth and divergent flow regimes.

The occurrence of concavities, or dimples, in the axial velocity profiles for inelastic tube entry flow have been observed and predicted. Experimental observations for Newtonian fluids (Burke and Berman, 1969; Uebler, 1966) confirm theoretical predictions (for example, Christiansen et al., 1972) that velocity profiles at the small tube entrance exhibit small concavities (less than 10%) at high Reynolds numbers. Similarly, Duda and Vrentas (1973) predict off-center maxima in the entry profile for the creeping flow of highly shear thinning inelastic fluids. However, concavities of the type shown in Figures 7 and 8, one and one half tube radii upstream of the contraction plane, with a maximum velocity near the wall three to five times greater than the local minimum at the center line, have never before been predicted or observed in laminar entry flow.

Several authors have conjectured that the development of inflection points in velocity profiles can lead to potentially unstable flows. Joseph (1964) has found that plane Poiseuille flow can develop concave profiles which are inviscidly unstable. Inflection points can also develop in pipe flows, but no instability was predicted in this case. Dealy (1964) has suggested that the existence of off-center maxima can have an important effect on the stability of the flow. It is well known that the high Reynolds number pipe flow of Newtonian fluids is unstable (turbulence). Duda and Vrentas (1973) speculated that the limited stability of concave velocity profiles is partially responsible for this and for the low Reynolds number instabilities observed in highly shear, thinning viscoelastic fluids. This subject will be reconsidered in Part III, where unstable laminar entry flow will be examined.

A final qualitative comparison of the kinematic characteristics of the two flow regimes is given in Figure 9. The rearrangement of axial velocity profiles through the entry region is schematically shown in normalized form for the vortex growth and divergent flow situations. For the vortex growth case, the location of maximum velocity at every axial position is the tube center line. The bulk of the fluid enters the small tube via a narrow convergent section about the tube center line. In divergent flow, the locus for the maximum velocity moves away from the center line, towards the tube wall, as the vortex detachment plane is approached. Within the vortex region, the greater part of the fluid approaching the small tube entrance does so via a small annular ring near the vortex boundary, and the flow near the center line approaches a semistagnant condition. Again, the image of an invisible obstacle to the flow at the tube center line near the detachment plane is useful.

A KINEMATIC MODEL FOR THE VORTEX GROWTH REGIME

A number of kinematic models for viscoelastic entry flow have been proposed in the literature. Metzner et al. (1969) approximated the kinematics for a reentrant tube to that of purely radial sink flow. Pickup (1970) found that the center-line velocity upstream of a slit entry was approximately an exponential function of axial distance from the slit.

In the model to be proposed here for the vortex growth regime, consideration is given to the shape of the axial velocity profiles in the entry region, as shown schematically in the upper portion of Figure 9. Examination of the profiles suggests that a reasonable approximation to the kinematics may be to neglect the flow predevelopment upstream of the detachment plane and consider the normalized axial velocity profile to maintain its fully developed shape throughout the vortex region. Thus, acceleration only occurs in the region $-L_v \leq z \leq 0$. If an appropriate functional expression can be obtained for the shape of the vortex boundary, to obtain R_v as a function of z, then the convergent flow kinematics can be specified, using the assumption of fully developed flow throughout the entry region.

Consider the fully developed flow of a power law fluid in the upstream tube. The axial velocity profile is given by

$$\frac{v_z}{\langle v_z \rangle_u} = \left\{ \frac{3n+1}{n+1} \right\} \left\{ 1 - \left(\frac{r}{R_u} \right)^{\left(\frac{n+1}{n}\right)} \right\} \tag{3}$$

Similarly, in the downstream tube

$$\frac{v_z}{\langle v_z \rangle_d} = \left\{ \frac{3n+1}{n+1} \right\} \left\{ 1 - \left(\frac{r}{R_d} \right)^{\left(\frac{n+1}{n}\right)} \right\} \tag{4}$$

In the proposed model, the axial velocity profile in the vortex region maintains the fully developed form, as

$$\frac{v_z}{\langle v_z \rangle_v} = \left\{ \frac{3n+1}{n+1} \right\} \left\{ 1 - \left(\frac{r}{R_v} \right)^{\left(\frac{n+1}{n}\right)} \right\} \tag{5}$$

for

$$-L_v \leq z \leq 0$$

It remains to obtain a functional expression for R_v in terms of z, which satisfies the following conditions:

at

$$z = 0, \quad R_v = R_d \tag{6a}$$

and

$$\frac{dR_v}{dz} = 0 \tag{6b}$$

at

$$z = -L_v, \quad R_v = R_u \tag{6c}$$

Condition (6b) is dictated by the evidence that the vortex boundary is parallel to the tube center line at the small tube entrance (see Figure 7 in Part I, for example).

The function form chosen was

$$R_v = R_d \exp\left\{ A^2 \left(\frac{z}{L_v} \right)^2 \right\} \tag{7}$$

This expression satisfies conditions (6a) and (6b). Moreover, substitution of condition (6c) into Equation (7) yields

$$A = \sqrt{\ln \beta} \tag{8}$$

The functional expression for R_v in Equations (7) and (8) gives remarkably good agreement with the experimentally observed vortex shapes in the 4:1 contraction. This is illustrated in Figure 10a for cases V3.1 and V3.2.

The advantage of the functional expression in Equations (7) and (8) is that it contains only the contraction ratio and the vortex length as parameters. The vortex length was shown in Part I to be directly proportional to N_{WS} in the vortex growth regime, independent of contraction ratio (Figure 14 in Part I). The relationship between L_v and N_{WS} (based on downstream conditions) was observed in Part I to be

$$L_v = 5\, R_u N_{WS} \tag{9}$$

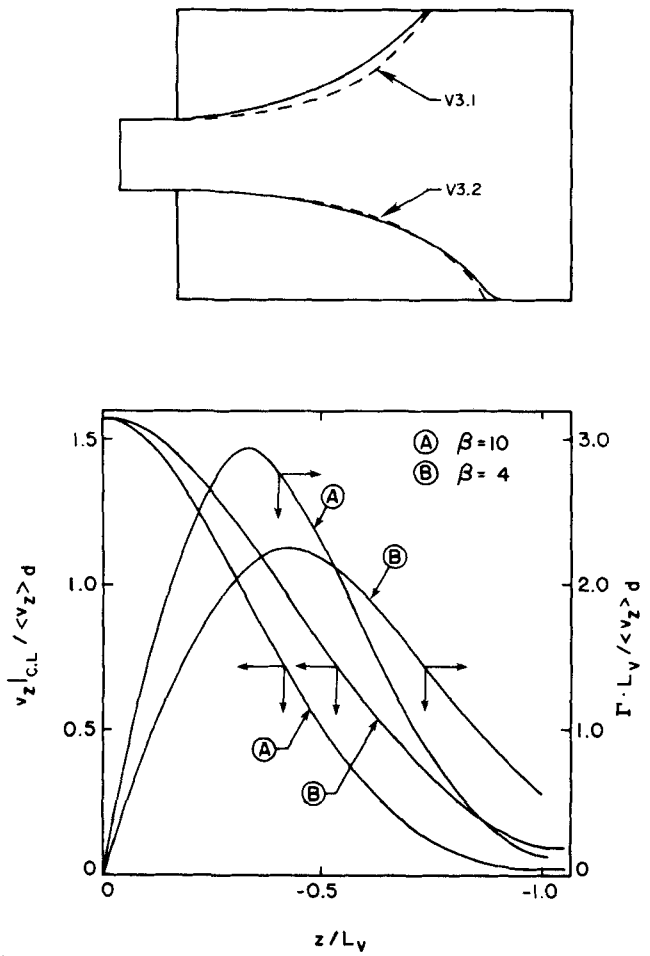

Fig. 10. Vortex shapes, center-line velocities, and stretch rates predicted by the kinematic model for the vortex growth regime. *(a)* Predicted vortex shapes in 4:1 contraction (dotted lines) compared to experimntally observed shapes (solid lines) for V3.1 and V3.2. *(b)* Dimensionless center-line velocity and stretch rate in the vortex region for two contraction ratios.

This may be used in Equation (7) to specify R_v in terms of β, R_d, N_{WS}, and z.

The mean velocity in the vortex region is found by combining Equations (7) and (2) as

$$\langle v_z \rangle_v = \langle v_z \rangle_d \exp\left\{ -2A^2 \left(\frac{z}{L_v} \right)^2 \right\} \tag{10}$$

Substituting Equations (7) and (10) into (5) specifies the velocity profiles through the converging flow field as

$$v_z = \left(\frac{3n+1}{n+1} \right) \frac{\langle v_z \rangle_d}{f_v^2} \left[1 - \left(\frac{r}{R_d \sqrt{f_v}} \right)^{\frac{n+1}{n}} \right] \tag{11}$$

where

$$f_v = \frac{R_v^2}{R_d^2} = \exp\left\{ 2A^2 \left(\frac{z}{L_v} \right)^2 \right\} \tag{12}$$

Equations (11) and (12) describe the accelerating axial velocity profiles for the vortex growth regime in terms of downstream conditions, the contraction ratio, and the vortex length [or N_{WS} from Equation (9)], and axial and radial coordinate positions. The radial velocity profiles have not been specified but are of secondary importance for the present purpose.

Using the approximate kinematic model, some interesting results may be derived. Consider the axial velocity at the center line:

$$v_{zC\cdot L} = \left(\frac{3n+1}{n+1} \right) \langle v_z \rangle_d \exp\left\{ -2A^2 \left(\frac{z}{L_v} \right)^2 \right\} \tag{13}$$

The axial velocity gradient or stretch rate at the center line is

$$\Gamma = \left. \frac{\partial v_z}{\partial z} \right|_{c\cdot L}$$

Differentiating Equation (13), we get

$$\Gamma = -\left(\frac{3n+1}{n+1} \right) \frac{4A^2 \langle v_z \rangle_d z}{L_v^2 \cdot f_v} \tag{14}$$

The function in Equation (14) attains a maximum value at

$$\frac{z_{\max}}{L_v} = -\frac{1}{2A} \tag{15}$$

and the maximum value is

$$\Gamma_{\max} = 1.213 \left(\frac{3n+1}{n+1} \right) \frac{A \langle v_z \rangle_d}{L_v} \tag{16}$$

The variation with axial position of the center-line velocity [Equation (13)] and the center-line stretch rate [Equation (14)] is illustrated in dimensionless form in Figure 10*b*, for $\beta = 4$ and $\beta = 10$, and $n = 0.40$. It is apparent that the maximum dimensionless stretch rate, expressed as $(\Gamma_{\max} \cdot L_v / \langle v_z \rangle_d)$, increases with β, and the axial position for $\Gamma = \Gamma_{max}$ approaches the contraction plane as β increases. Using the experimental conditions for cases V3.1 and V3.2 (Table 1), the maximum stretch rate and its location were calculated for these two situations, using Equations (15) and (16). The resulting data points are compared with the experimentally determined stretch rates in Figure 4. The agreement between the predicted and observed values for $\Gamma_{\max}$ and $z_{\max}$ is reasonable.

The maximum extension rate in the entry flow region is of interest because some authors have predicted that a critical extensional rate exists in homogeneous steady extension, above which the stress response of certain fluids to the deformation field is unbounded (for example, Denn and Marrucci, 1971; Everage and Gordon, 1971). Everage and Ballman (1974) have identified the product of fluid relaxation time θ with extensional rate Γ as a recoverable strain. Using Equation (16), we get

$$\theta \Gamma_{\max} = 1.213\, A \left(\frac{3n+1}{n+1} \right) \left(\frac{\langle v_z \rangle_d}{L_v} \right) \tag{17}$$

If the fluid relaxation time in Equation (17) is evaluated at the downstream wall shear rate, then the last term in Equation (17) may be substituted by N_{WS}/X, yielding

$$\theta \Gamma_{\max} = \frac{1.213\, A}{\beta} \left(\frac{3n+1}{n+1} \right) \cdot \left(\frac{N_{WS}}{X} \right) \tag{18}$$

It has been established that the parameter N_{WS}/X is constant in the vortex growth regime and that it may be interpreted as a macroscopic Deborah number. Thus, it is suggested by the kinematic model that an additional characteristic of the vortex growth regime is that the maximum recoverable extensional strain in the entry region remains essentially constant. Moreover, the maximum extensional strain may be estimated quite simply using the kinematic model and steady shear flow measure-

TABLE 2. DEBORAH NUMBERS IN THE VORTEX GROWTH REGIME

Case	θ_w (s)	T_{vortex} (s)	N_{De}
V3.1	0.0173	0.61	0.028
V3.2	0.0125	0.44	0.028

ments (to obtain N_{WS}). This is an important conclusion. Everage and Ballman (1974) have suggested that the correlation of entry flow behavior with steady shear flow measurements is erroneous. They suggest that the recoverable extensional strain ($\theta\Gamma$) is of vital importance in correlating the onset of unstable flow. Equation (18) shows that the extensional criterion can be derived from steady shear flow measurements. The concept of a critical value of the recoverable extensional strain is equivalent to that of a critical Deborah number for the flow.

A more rigorous interpretation of N_{WS}/X as a Deborah number is obtained by estimating the time spent by a fluid particle in the accelerative region of the entry zone. If we consider a particle at the tube center line, the residence time in the changing deformation field is given by

$$T_{vortex} = \int_{-L_v}^{0} \frac{dz}{v_z|_{C\cdot L}} \tag{19}$$

Substituting Equation (13) for $v_z|_{C\cdot L}$ in Equation (19), we get

$$T_{vortex} = \frac{L_v}{\langle v_z \rangle_d} \left(\frac{n+1}{3n+1} \right) I(\beta) \tag{20}$$

where the integral term

$$I(\beta) = \frac{1}{A\sqrt{2}} \int_{-A\sqrt{2}}^{0} e^{x^2} dx \tag{21}$$

is a function only of the contraction ratio. For $\beta = 2$, $I = 2.05$, and for β, $I = 4$, $I = 6.11$. Defining the characteristic Deborah number for the flow as a ratio of characteristic fluid and process times

$$N_{De} = \frac{\theta_{fluid}}{T_{vortex}} \tag{22}$$

and substituting for T_{vortex} from Equation (20), we get

$$N_{De} = \frac{\theta \langle v_z \rangle_d}{L_v} \cdot \left(\frac{3n+1}{n+1} \right) \cdot \frac{1}{I(\beta)} \tag{23}$$

If the value for the fluid relaxation time θ in Equation (23) is evaluated at the downstream wall shear rate, then the parameter N_{WS}/X may be introduced. The result is

$$\frac{N_{WS}}{X} = \beta I(\beta) \left(\frac{n+1}{3n+1} \right) \cdot N_{De} \tag{24}$$

Equation (24) confirms the earlier interpretation of N_{WS}/X as a true Deborah number, based on secondary vortex considerations.

Values for the Deborah number in Equation (23) were calculated for fluid V3 in the 4:1 contraction using the conditions in Table 1, and the experimentally determined values for L_v. The calculation of T_{vortex} follows directly from Equation (20). Table 2 summarizes the relevant parameters for the two cases studied in the vortex growth regime.

The results in Table 2 offer partial justification that the vortex growth regime is a constant Deborah number flow. The constant value of $N_{De} = 0.028$ is based on experimental measurements of $\langle v_z \rangle_d$, θ, L_v, and n.

ACKNOWLEDGMENT

The experimental measurements for this paper were made in the Department of Chemical Engineering, Monash University, where the work was supported by a grant from the Australian Research Grants Commission. The paper was compiled at the Department of Chemical Engineering, University of Delaware. The seond author is particularly grateful to the Delaware department for the support and encouragement received.

NOTATION

A = parameter in kinematic model, Equation (18)
f_v = vortex radius factor, Equation (12)
$I(\beta)$ = integral defined by Equation (21)
L_v = vortex detachment length
N_1 = first normal stress difference
N_{De} = Deborah number
N'_{Re} = modified Reynolds number
N_{WS} = Weissenberg number
n = power law index
Q = volumetric flow rate
R_d = radius of downstream tube
R_u = radius of upstream tube
R_v = radius of converging flow
r = radial spacial coordinate
T_{vortex} = residence time of a fluid particle in the entry region
v_r = radial velocity component
v_z = axial velocity component
$\langle v_z \rangle$ = average axial velocity
$v_z|_{C\cdot L}$ = axial velocity at center line of tube
$v_z|_N$ = normalized axial velocity, Equation (1)
z = axial spacial coordinate
Γ = center-line stretch rate
Γ_{max} = maximum center-line stretch rate
γ = shear rate
θ = Maxwell relaxation time

Subscript

w = condition at downstream tube wall

LITERATURE CITED

Burke, J. P., and N. S. Berman, "Entrance Flow Development in Circular Tubes at Small Axial Distances," ASME paper No. 69-WA/FE-13 (1969).

Christiansen, E. B., S. J. Kelsey, and T. R. Carter, "Laminar Tube Flow Through an Abrupt Contraction," *AIChE J.*, **18**, No. 2, 372-380 (1972).

Denn, M. M., and G. Marrucci, "Stretching of Viscoelastic Liquids," *ibid.*, **17**, No. 1, 101-103 (1971).

Duda, J. L., and J. S. Vrentas, "Invisid Flow Through a Sudden Contraction," *Ind. Eng. Chem. Fundamentals*, **11**, No. 4, 590-593 (1972).

Everage, A. E., and R. J. Gordon, "On the Stretching of Dilute Polymer Solutions," *AIChE J.*, **17**, No. 5, 1257-1259 (1971).

Everage, A. E., and R. L. Ballman, "A Mechanism for Polymer Melt or Solution Fracture," *J. Appl. Polymer Sci.*, **18**, 933-957 (1974).

Metzner, A. B., E. A. Uebler, and C. F. Chan Man Fong, "Converging Flows of Viscoelastic Materials," *AIChE J.*, **15**, No. 5, 750-758 (1969).

Metzner, A. B., J. L. White, and M. M. Denn, "Constitutive Equations for Viscoelastic Fluids for Short Deformation Periods and for Rapidly Changing Flows: Significance of the Deborah Number," *ibid.*, **12**, No. 5, 863-866 (1966).

Pickup, T. J. F., "Converging Flow of Viscoelastic Fluids," Ph.D. thesis, Cambridge Univ., London, England (1970).

RamaMurthy, A. V., "Laminar Flow of Viscous and Viscoelastic Fluids in the Entrance Region of a Pipe," Ph.D. thesis, Monash Univ., Clayton, Victoria, Australia (1970).

Manuscript received April 4, 1977; revision received and accepted March 27, 1978.